Acta Metallurgica Sinica (English Letters) (2022) 35:1765–1776
https://doi.org/10.1007/s40195-022-01405-7

# Wear Behavior of the Uniformly Dispersed Carbon Nanotube Reinforced 6061Al Composite Fabricated by Milling Combined with Powder Metallurgy

Xiaonan Li[1,2] · Zhenyu Liu[2] · Zhixin Dai[1,2] · Hui Feng[2] · Bolyu Xiao[2] · Dingrui Ni[2] · Quanzhao Wang[2] · Dong Wang[2] · Zongyi Ma[2]

Received: 1 December 2021 / Revised: 2 January 2022 / Accepted: 10 January 2022 / Published online: 28 April 2022


**Abstract**
The uniformly dispersed carbon nanotubes (CNTs) reinforced 6061Al composites (CNT/6061Al) with different CNT concentrations were fabricated by powder metallurgy technology. It was found that the friction coefficient as well as wear rate decreased first and then increased as the CNT concentration increasing under 15 N as well as 30 N, and the minimum wear rate was achieved at the CNT concentration of 2 wt%. Adhesive wear and abrasive wear were the dominated wear mechanisms for the 1–2 wt% CNT/6061Al composites under 15 N and 30 N, while the delamination occurred on the wear surface at 3 wt% CNT. As the applied load increased to 60 N, the wear rate of composites increased dramatically. The wear mechanism transformed from abrasive wear to severe delamination wear, accompanied by the generation of wear debris with sharp edge due to the weaker anti-shearing strain capacity of CNT/6061Al composites.

**Keywords** Wear mechanism · Carbon nanotube · Aluminum matrix composites · Powder metallurgy

## 1 Introduction

Carbon nanotube (CNT) reinforced aluminum matrix (CNT/Al) composite has drawn extensive concern due to its lower density, higher modulus (~ 1 TPa) and higher strength (~ 30 GPa). Until recently, a great deal of research work has been focused on composite preparation [1, 2], structure design [3–5] and tensile property [6–9]. Moreover, the extraordinary electrical and thermal properties of CNT make the CNT/Al composites potential materials for the application of current-carrying parts (e.g., armature in the electric contact field). However, the severe wear between Al base materials and wear counterpart was the main obstacle to the applications for aluminum base materials in the electric contact field.

Some studies have examined the wear resistance of CNT/Al composites [10–16]. Bastwros et al. [14] found that the wear rate decreased significantly with the increase of CNT concentration for the generation of carbon film during friction condition. Choi et al. [10] illustrated that the CNT dispersion lead in the grain refinement, which also contributed to enhancing wear property. However, Yildirim et al. [17] pointed out that the wear rate decreased first and then increased with the increased of CNT concentration. These controversial results might attribute to the CNT cluster in the mentioned investigations, because the CNT dispersions in the composites were not mentioned and the actual dispersion state of CNT could only be speculated according to the reported preparation methods and experimental results. This complicated the relationship of CNT distribution and wear behaviors. Overall, the wear behavior of CNT/Al composites was still not clear enough.

Under some special service conditions, the adhesion between metal and counterpart was a mainly considered problem [18–21], especially for the electric contact field. Aluminum was easier to cause adhesion wear for its higher average adhesion coefficient, as compared with copper or

Available online at http://link.springer.com/journal/40195.

✉ Zhenyu Liu
zyliu@imr.ac.cn

[1] School of Materials Science and Engineering, University of Science and Technology of China, Shenyang 110016, China

[2] Shi-Changxu Innovation Center for Advanced Materials, Institute of Metal Research, Chinese Academy of Sciences, Shenyang 110016, China

iron [22]. Ferrante et.al [23] summarized the results of adhesion experiment on copper–aluminum alloys with a gold (111) single crystal, indicating that even a small percentage of aluminum in these alloys could dramatically increase the adhesive properties as compared with pure copper, and its bonding force rapidly approached that of pure aluminum.

According to the existed reports on the wear behaviors of CNT/Metal composites, the alumina [10, 12], SiC paper [11], steel [14–17, 24] were usually chosen as the counterpart material, which inhibited the adhesion wear due to the high cohesive strength [25]. In the actual electrical field, Cu base material was widely used. However, it had a much higher average adhesion coefficient as compared with that of iron, which means that the adhesion wear between Al and Cu might be serious. To the best of our knowledge, there were no researches on the wear behavior of CNT/Al composite using the Cu base material as the counterpart. Thus, it was necessary to investigate the wear behavior of CNT/Al composite against the Cu base counterpart.

In this study, the well dispersed CNT/6061Al composites were prepared through high energy milling (HEM) combined with powder metallurgy technology. The CNT distribution, hardness and wear behavior of CNT/6061Al composites against the albronze counterpart were examined. The aim of the present work was to study the effect of CNT concentration and loading on the wear behavior of CNT/6061Al composites under the higher adhesion coefficient system.

## 2 Experimental

### 2.1 Raw Materials and Composite Fabrication

The as received CNT (Fig. 1a) synthesized using chemical vapor deposition had an outer diameter of 10–20 nm and a length of ~ 5 $\mu$m, with purity higher than 98%. The as received 6061Al powders had a chemical composition of Al–1.2 wt% Mg–0.6 wt% Si–0.2 wt% Cu, with an average diameter of about 13 $\mu$m (Fig. 1b). The CNT/6061Al composites were prepared through HEM combined with powder metallurgy technology. Firstly, CNTs with different concentrations (1–3 wt%) were respectively milled with 6061Al powders in an attritor for 6 h, and conducted at a rotational speed of 400 RPM with a ball powder ratio of 15:1. Secondly, the milled CNT/6061Al powders were respectively cold-compacted into a cylinder die, degassed and hot pressed at 853 K for 1 h. Then, the as-hot pressed billets were hot extruded at 723 K with an extrusion ratio of 16:1. Finally, the CNT/6061Al composites were solution treated at 803 K for 2 h, quenched into water at room temperature and then artificial aged at 443 K for 6 h (i.e., T6 treatment). For comparison, 6061Al alloy was also fabricated under the same preparation and heat treatment conditions.

### 2.2 Wear Tests and Characterization of the CNT/6061Al Composites

Wear tests for the CNT/6061Al were performed using a pin-on-disk type wear tester (MM-W1A vertical friction and wear testing machine) at room temperature. The wear samples of CNT/6061Al composites were sectioned along the hot extrusion direction and machined into cylindrical pins with a diameter of 4.7 mm and height of 15 mm. Albronze annular disks with an average hardness of 253 HV were chosen as the wear counterparts. Both of the cylindrical pin and counterpart surface were polished with 1000 mesh SiC paper and then degreased with acetone before testing. The tests were carried out under dry sliding condition at a constant sliding speed of 0.5 m/s, constant sliding distance of 600 m under different applied loads of 15, 30 and 60 N, respectively. The wear rates of CNT/6061Al composites were determined by the following equation:

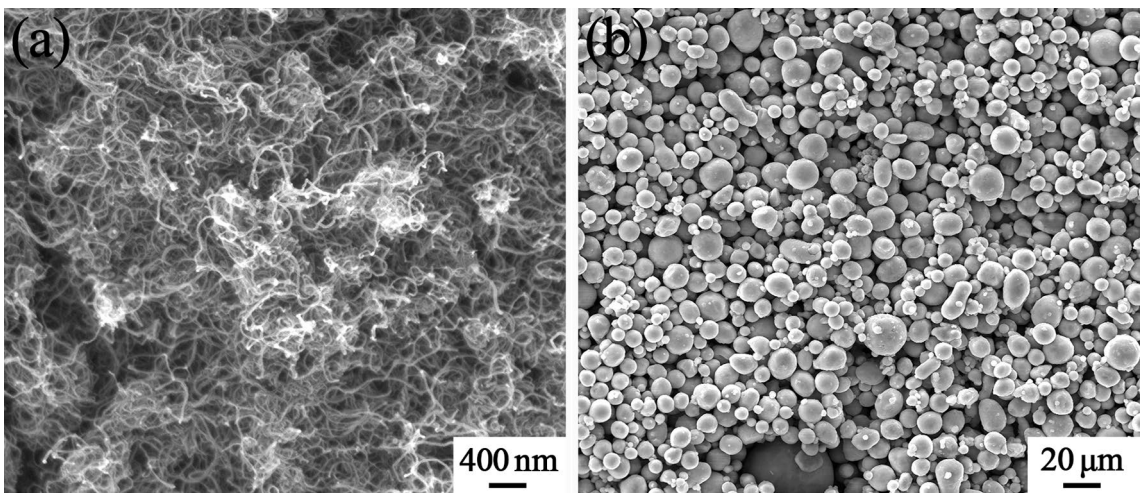


**Fig. 1** SEM images of the as-received **a** CNT, **b** 6061Al powders

$$K = \frac{\Delta m}{\rho \cdot L},$$

where $K$ ($mm^{-3}\ m^{-1}$) is the wear rate, $\Delta m$ (g) is the mass loss of composite sample after the wear test, $\rho$ ($g\ cm^{-3}$) is the density of composite, $L$ (m) is the sliding distance. The weight of the specimens before and after the wear tests were measured using a digital balance with an accuracy of 0.001 mg.

The hardness was measured 10 times with a Vickers hardness tester (FM-700, a load of 200 g and a dwell time of 15 s) to obtain the average value. A transmission electron microscope (TEM, Tecnai G2 20) was used to examine the CNT distribution of CNT/6061Al composites. Scanning electron microscopy (SEM, Inspect F50) with energy-dispersive spectroscopy facility was used to characterize the wear surface, cross section of the wear samples, counterpart surfaces and wear debris. The 3D morphologies of the wear surfaces were examined by a surface mapping microscope (3D Micro XAM, KLA, USA). The CNT strain states on the wear surfaces were characterized by a micro-Raman spectroscopy unit (Jobin Yvon HR800) with a laser wavelength of 532 nm and power of 3.2 mW.

## 3 Results and Discussion

### 3.1 Structure of Grain and Precipitation Phase

The microstructures of CNT/6061Al composites with different CNT concentrations are shown in Fig. 2. It can be seen that the grains of CNT/6061Al composites (Fig. 2a–d) were elongated slightly as the result of hot extrusion deformation, and the grains were refined gradually with the increase in CNT concentration, which was a common phenomenon in CNT/Al composites. Further, many needle-shape nanoprecipitates ($\beta''$), which were common precipitate phase in Al–Mg–Si series alloy, could be seen in all composites (Fig. 2e–h). It should be mentioned that, the precipitates shape, size and distribution did not show significant differences, with increasing CNT concentration.

### 3.2 CNT Distribution and Vickers Hardness of CNT/6061Al Composites

Figure 3a shows the distribution of CNTs in the 3 wt% CNT/6061Al composite along the extrusion direction. On the whole, no obvious agglomeration of CNT could be observed and CNT were individually dispersed in the Al matrix, which mainly attributed to the repeated deformation, cold welding and fracture processes during HEM [26, 27]. With increasing CNT concentration, the Vickers hardness increased significantly as the result of the strengthening induced by the uniformly dispersed CNTs and grain refinement [28], while the elongation of CNT/6061Al composites decreased (Fig. 3b).

### 3.3 Friction Coefficient and Wear Rate

Figure 4 shows the friction coefficient curves of CNT/6061Al composites with different CNT concentrations

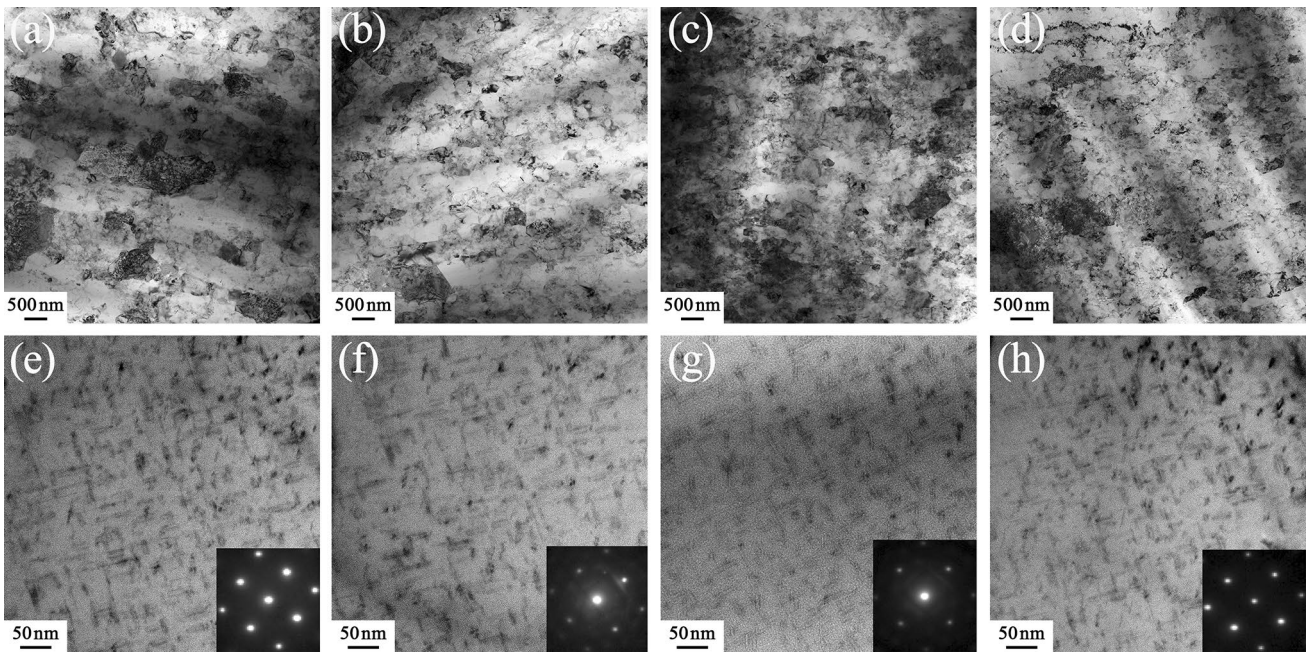


**Fig. 2** TEM images showing the grain and precipitation phase of CNT/6061Al composites with different CNT concentrations: **a**, **e** 0 wt%, **b**, **f** 1 wt%, **c**, **g** 2 wt%, **d**, **h** 3 wt%

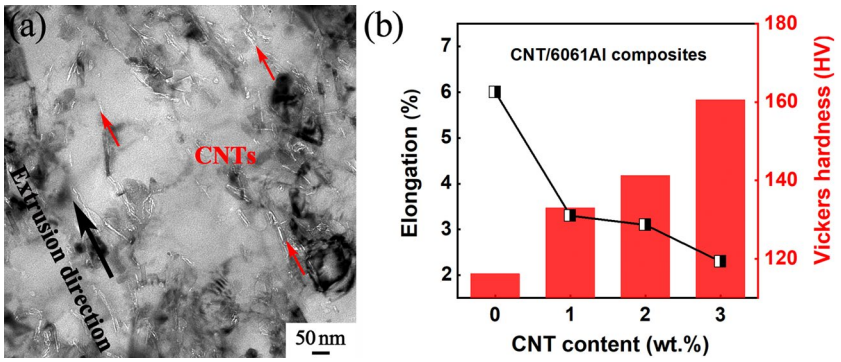


**Fig. 3** **a** TEM image of individually dispersed CNTs in the 3 wt% CNT/6061Al composite; **b** Vickers hardness and elongation of CNT/6061Al composites with different CNT concentrations

under different applied load of 15 N, 30 N and 60 N, respectively. It can be seen that the friction coefficient curves under 15 N showed a large fluctuation (Fig. 4a), and the friction coefficient curves became smoother as the load increased to 30 N (Fig. 4b). However, the fluctuation of the friction coefficient at the initial stage was large and then tended to smooth under the applied load of 60 N (Fig. 4c).

The friction coefficient changing curves of CNT/6061Al composites under different applied load are shown in Fig. 5a. The friction coefficient curves under 15 N and 30 N showed similar changing trend with increasing CNT concentration. The composites with 1 wt% CNT achieved the lowest friction coefficient, and then the friction coefficient increased apparently with the increase in CNT concentration. However, the friction coefficient decreased gradually with the increase in CNT concentration under the applied load of 60 N, and it reached the lowest friction coefficient as the CNT concentration increased to 3 wt%. This phenomenon was also found in many metal pairs under the high load. The very smooth surfaces and a large quantity of wear debris were believed to be responsible for the friction coefficient decrease [29–31].

The wear rate changing curves under 15 N, 30 N and 60 N are shown in Fig. 5b. Under the applied load of 15 N and 30 N, the wear rate decreased slightly first and then increased rapidly as the CNT concentration increased from 0 to 3 wt%, which was also observed by Jiang et al. [15] under a relative lower load of 1 N and 3 N. One thing should be mentioned that, the wear rates of the CNT/6061Al composites in this study reduced by about four fifths under the same applied load of 15 N, as compared with those of the CNT/6061Al composites with CNT clustering in our previous study [32]. The significantly increased wear resistance was believed to originate from the individually dispersed CNTs.

As the applied load increased to 60 N, the wear rate increased dramatically, as compared to those under 15 N or 30 N. Further, the wear rate increased continuously as incresing the CNT concentration from 0 to 3 wt% under 60 N, which was quite different from those under 15 N and 30 N. Until recently, no relevant wear behavior under such high applied load have been reported.

The wear rate of the counterpart materials was also examined (Fig. 5c). It can be clearly seen that the wear rate of counterpart material gradually decreased with increasing CNT concentration under any applied load. Especially, under the applied load of 60 N, the wear rate decreased significantly with increasing CNT concentration. This

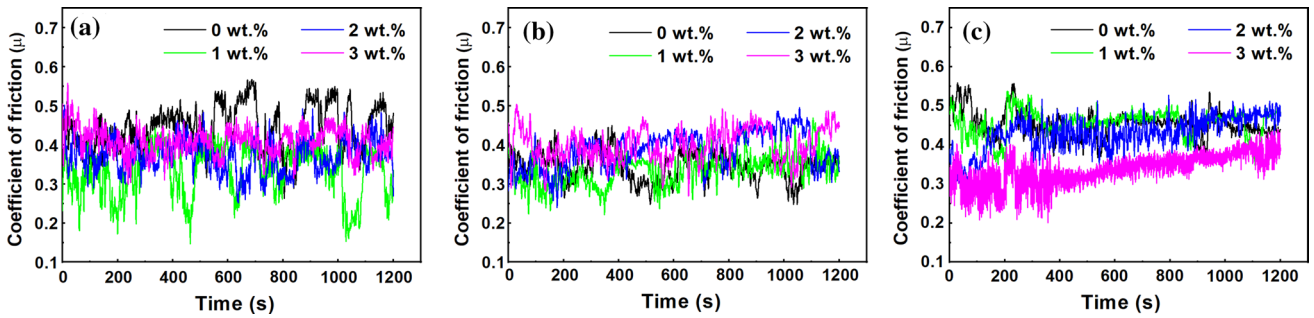


**Fig. 4** Friction coefficient versus the sliding time for the CNT/6061Al composites with different CNT concentrations under **a** 15 N, **b** 30 N, **c** 60 N

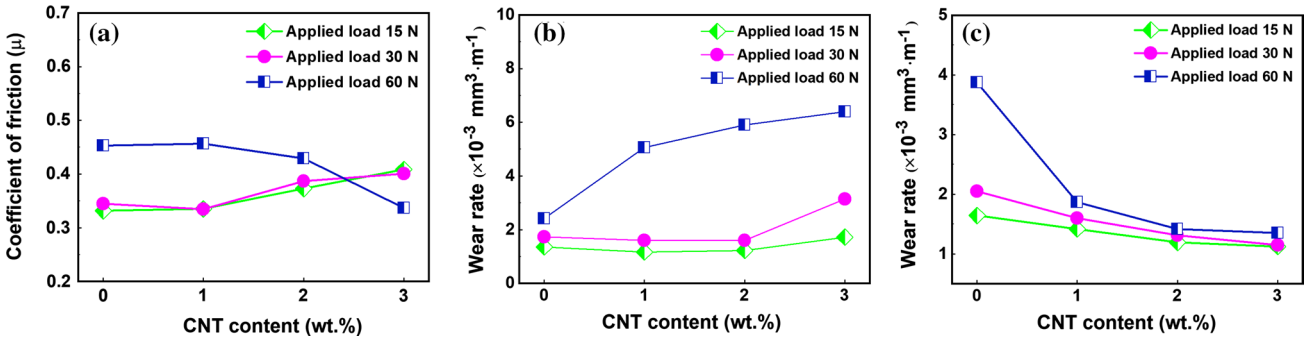


**Fig. 5** **a** Friction coefficient, **b** wear rate of CNT/6061Al composites, **c** wear rate of counterpart material under different applied loads and CNT concentrations

indicates the incorporation of CNT could effectively protect the counterpart.

### 3.4 Characters of Wear Surfaces

Figure 6 shows the typical wear surface morphology of CNT/6061Al composites with different CNT concentrations under 30 N and 60 N. It was found that many counterpart materials (the bright color) adhered to the wear surface (Fig. 6a–d). In general, the material transfer was preferential from the flat disk to the pin for a pin-on-disk system, unless the unworn disk was much harder than the unworn pin [25, 33]. As the result of the lower hardness and weaker cohesive strength of albronze as compared with those using alumina, SiC paper or high strength steel [21, 25, 34], the material transfer from the counterpart to the pin was relatively easier in the wear process. Further, many grooves could be observed on the wear surface of CNT/6061Al samples, which was the typical characteristic of abrasive wear. As the applied load increased to 60 N, the grooves (Fig. 6e–h) decreased gradually with the increase in CNT concentration.

Figure 7 shows the magnified wear surface morphology of CNT/6061Al composites with different CNT concentrations under an applied load of 30 N. The ploughing grooves and microcracks could be observed on the wear surfaces (Fig. 7a–c). As the CNT concentration increased from 0 to 2 wt%, the number of microcracks decreased gradually (Fig. 7e–g). As the CNT concentration further increased to 3 wt%, the number and size of microcracks increased dramatically. It is believed that the subsurface deformation under repeated loading was the principal

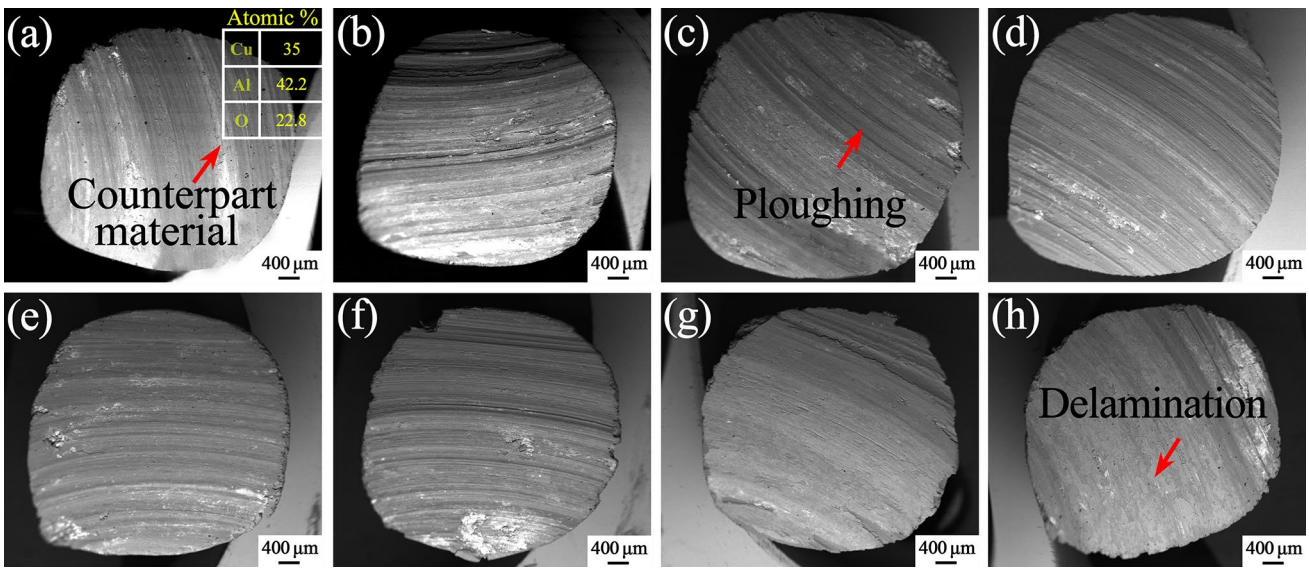


**Fig. 6** SEM images showing the wear surface morphology of CNT/6061Al composites with different CNT concentrations under 30 N: **a** 0 wt%, **b** 1 wt%, **c** 2 wt%, **d** 3 wt%, 60 N: **e** 0 wt%, **f** 1 wt%, **g** 2 wt%, **h** 3 wt%

reason for the generation of microcracks. As the microcracks propagated to the surface (at certain weak positions), long and thin wear sheets (delamination) generated [35, 36]. This means that the microcracks with larger size and number would cause severe delamination wear (Fig. 7h). According to the above analysis, the wear mechanism of the CNT/6061Al composites under 30 N were dominated by adhesion and abrasive wear, while the delamination wear occurred as the CNT concentration increased to 3 wt%.

Figure 8 shows the magnified wear surface morphology of the CNT/6061Al composites with different CNT concentrations under an applied load of 60 N. Both of the ploughing grooves and microcracks could be observed on the wear surface, however, the ploughing grooves gradually disappeared with increasing CNT concentration, as shown in Fig. 8c and d. In addition, with the increase in CNT concentration, the number of microcracks decreased gradually (Fig. 8f–h).

### 3.5 Characters of Counterpart and Wear Debris

The wear surface morphologies of the counterpart under different applied load are shown in Fig. 9. Many grooves and adhered CNT/6061Al composite materials (the dark color) were observed on the counterpart wear surface. The counterpart wear surfaces were relatively smooth under the low applied load of 30 N. But the grooves became deeper as the applied load increased to 60 N, and the adhered CNT/6061Al composite materials increased with increasing CNT concentration. These results were consistent with the wear rate change of counterpart material (Fig. 5c).

The CNT/6061Al composite materials adhered on the wear surface of counterpart induced a great degree of wear between Al-Al, which played an important role in inhibiting the wear loss of counterpart. It was known that Al and Al had a much higher adhesion-binding energy ~ $525 \times 10^{-3}$ J/m$^2$, which resulted in the severe wear of CNT/6061Al composites [19, 21, 25].

Figure 10 shows the SEM images of the wear debris under different applied load of 30 N and 60 N. For the CNT/6061Al composites, the counterpart material (the bright color) in the wear debris decreased gradually with the increase in CNT concentration, which was in accordance with the wear rate changing of counterpart (Fig. 5c). The wear debris size decreased first and then increased with the increase of CNT concentration under 30 N (Fig. 10a–d), and the 1 wt% CNT/6061Al composite achieved the minimum size of the wear debris. As the applied load increased to 60 N, the wear debris size increased significantly (Fig. 10d–h) compared with that of 30 N. On the other hand, the wear debris turned from flaky shape to irregular shape with increasing CNT concentration. The irregular shape of wear debris with sharp edge would cause severe delamination during the sliding process.

## 4 Discussion

### 4.1 Change of Friction Coefficient

In general, the shape and size of the wear debris, as well as the wear surface roughness could reflect the friction

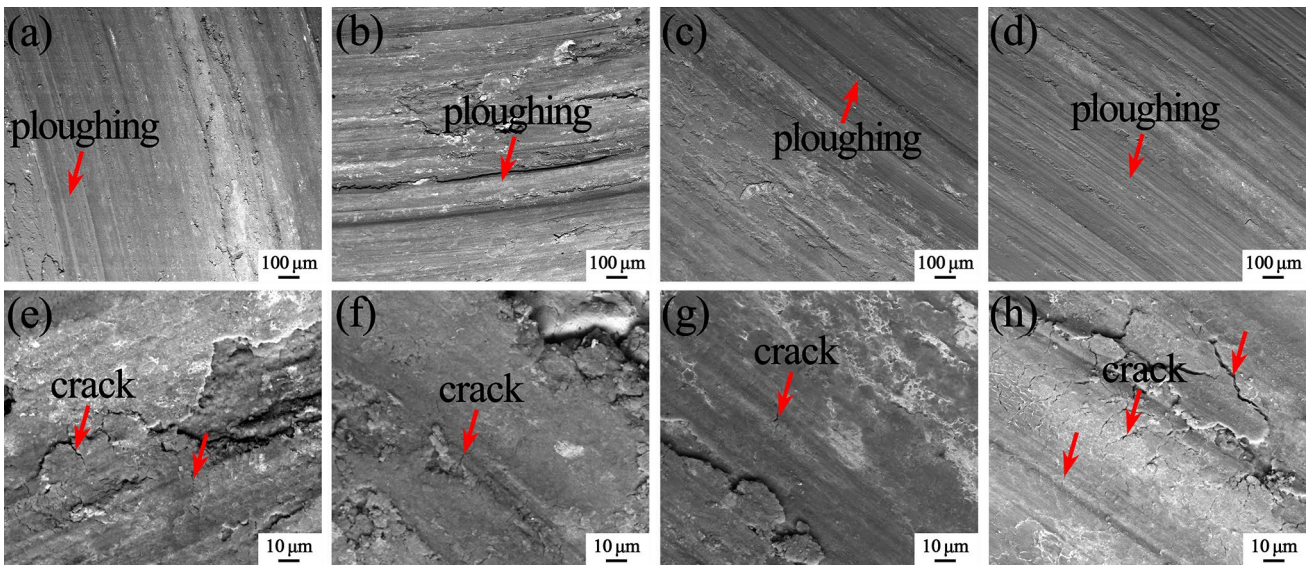


**Fig. 7** SEM images showing the wear surface morphology of CNT/6061Al composites with different CNT concentrations under 30 N: **a**, **e** 0 wt%, **b**, **f** 1 wt%, **c**, **g** 2 wt%, **d**, **h** 3 wt%

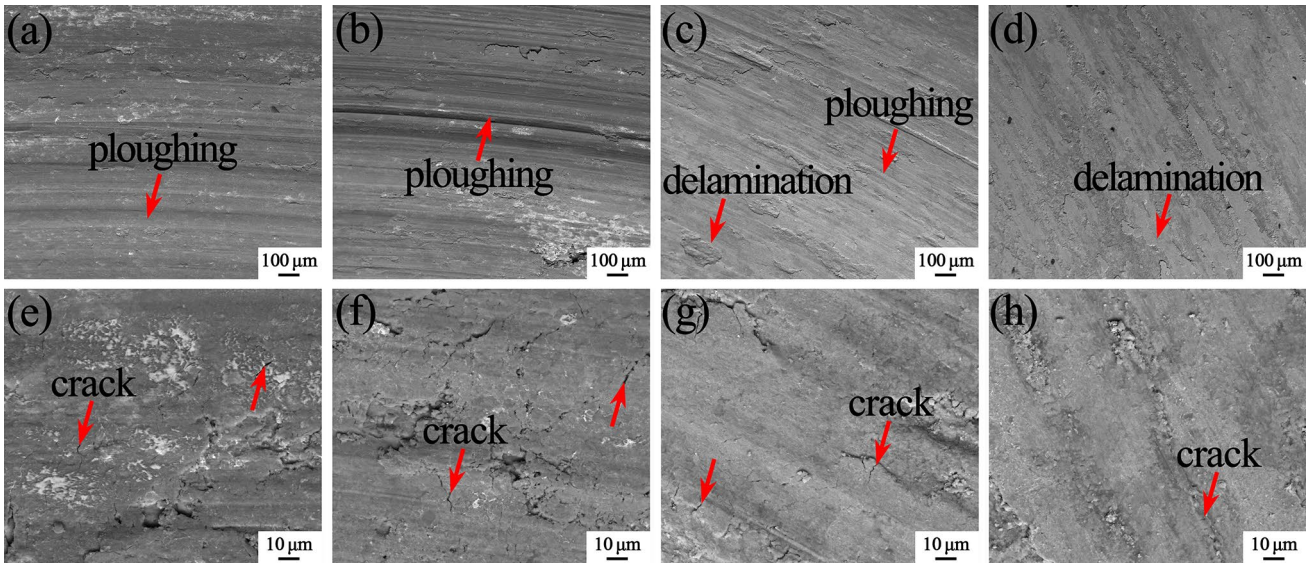


**Fig. 8** SEM images showing the wear surface morphology of CNT/6061Al composites with different CNT concentrations under 60 N: **a**, **e** 0 wt%, **b**, **f** 1 wt%, **c**, **g** 2 wt%, **d**, **h** 3 wt%

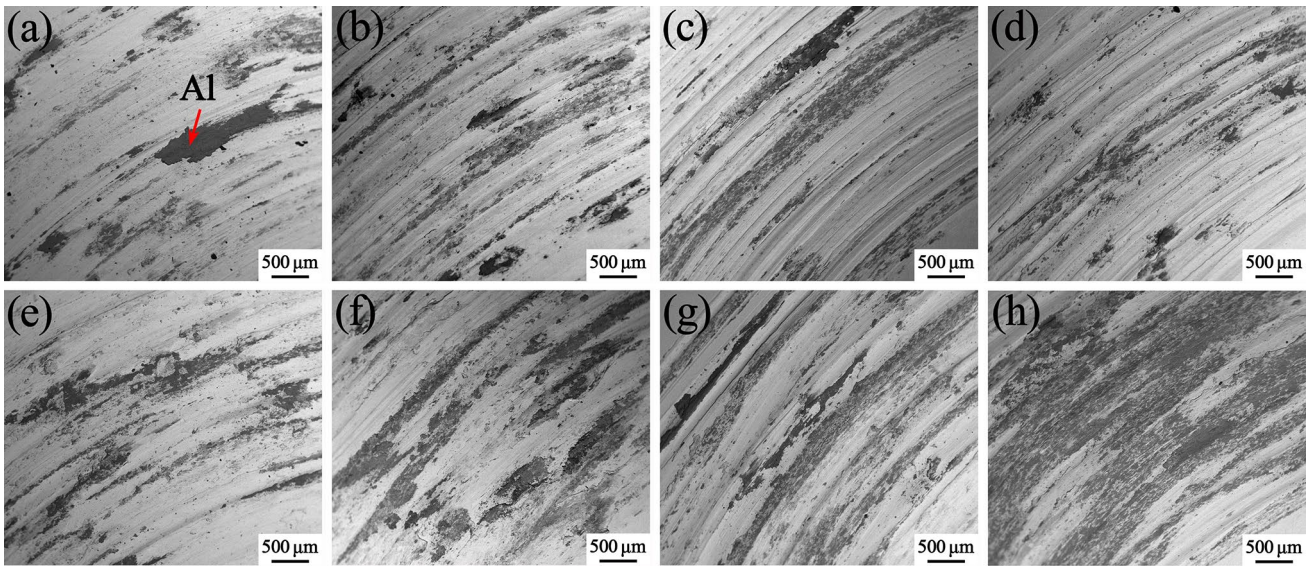


**Fig. 9** SEM images showing the wear surface morphology of counterparts for CNT/6061Al composites with different CNT concentrations under 30 N: **a** 0 wt%, **b** 1 wt%, **c** 2 wt%, **d** 3 wt%, 60 N: **e** 0 wt%, **f** 1 wt%, **g** 2 wt%, **h** 3 wt%

coefficient change to some extent. Previous studies have shown that the wear debris with smaller size and rounder shape was easier to roll between the dual wear surfaces, which usually resulted in a lower friction coefficient [37–39]. In this study, both of the wear debris size (Fig. 10a–d) and friction coefficient (Fig. 5a) decreased first and then increased under 30 N, as increasing the CNT concentration. Namely, they showed an approximate variation with the increase in CNT concentration.

For a better explanation of the variation of friction coefficient, the 3d profilograms of the wear surfaces and the change of *R*a (mean arithmetic deviation of surface roughness) values under 30 N are given (Fig. 11). As depicted in Fig. 11a–c, the grooves caused by ploughing could be detected, which was consistent with those observed

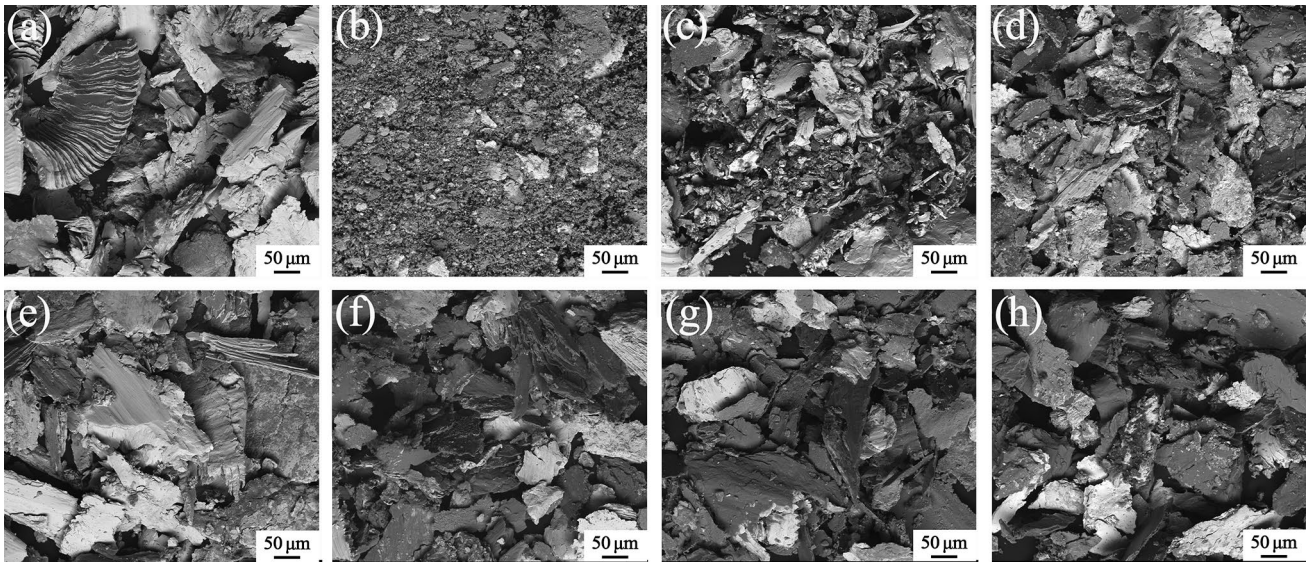


**Fig. 10** SEM images showing the wear debris morphology of the CNT/6061Al composites with different CNT concentrations under 30 N: **a** 0 wt%; **b** 1 wt%; **c** 2 wt%; **d** 3 wt%; 60 N: **e** 0 wt%; **f** 1 wt%; **g** 2 wt%; **h** 3 wt%

wear surface morphology in Fig. 6a–c. For the 3 wt% CNT/6061Al composite, the deeper and wider grooves were observed, which usually accompanied with severer wear. On the other hand, the value of *R*a decreased first and then increased with increasing CNT concentration, showing a similar variation tendency to that of the friction coefficient. This was in accordance with the previous finding that the higher value of *R*a usually accompanied with higher friction coefficient [40, 41].

The friction coefficient showed an inverse changing trend under 60 N, namely, the friction coefficient decreased gradually with increasing CNT concentration (Fig. 5a). As the applied load increased to 60 N, the wear debris size increased significantly as compared with that of 30 N (Fig. 10). But the size of wear debris decreased gradually as increasing the CNT concentration (Fig. 10d–h). Therefore, the friction coefficient increased significantly as compared with that under 30 N, but decreased gradually with the increase in CNT concentration. The 3d profilograms (Fig. 12) of the wear tracks under 60 N also gave a similar variation tendency of the roughness (*R*a) and the friction coefficient with increasing CNT concentration. This interesting phenomenon of friction coefficient change under 60 N was radically different from that reported by Kim et al. [13]. The possible reason for the increasing friction coefficient was the high shear stress under 60 N.

### 4.2 Effect of Mechanical Mixing Layer (MML) on Wear Behavior

Many studies [42–45] have demonstrated that the formation of MML could effectively slow down the wear process. For understanding the relationship of MML and wear behavior of CNT/6061Al composites, the wear subsurface cross sections of samples under different applied load of 30 N and 60 N were studied. It can be clearly seen that the MML formed on the wear surfaces of the CNT/6061Al composites under 30 N (Fig. 13). The thickness of MML gradually decreased with increasing CNT concentration, which weakened the wear of 1 wt% and 2 wt% CNT/6061Al composites to a certain extent. The magnified images indicate that the MML composed of fine debris, which fractured and comminuted continually from both sides of the contact surfaces (Fig. 13e–h). The generation process of MML was similar with those reported by Lee et al. [44] and Venkataraman et al. [45]. The alternate stacking of composites and counterpart materials was the chief reason for the generation of the MML.

Many microcracks could be observed in MML for 0 wt%, 2 wt% and 3 wt% CNT/6061Al composites, indicating a weaker adhesive strength of MML. Moreover, almost all of the microcracks initiated around the wear debris of albronze with bigger size. The larger microcracks also induced the generation of voids (Fig. 13h), which weakened the adhesive strength of MML. As a result, the wear rates of 6061Al and 3 wt% CNT/6061Al were higher than those of 1–2 wt% CNT/6061Al (Fig. 5b).

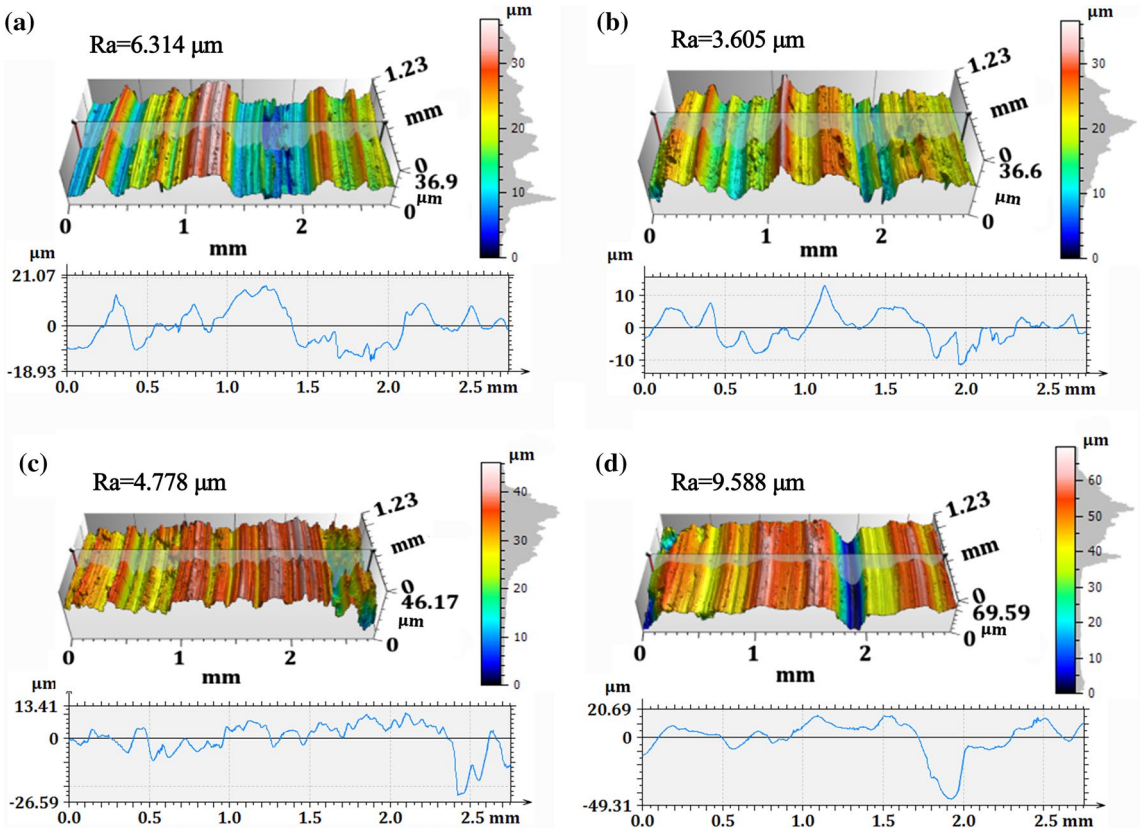


**Fig. 11** 3D profilogram of wear tracks for the CNT/6061Al composites with different CNT concentrations under 30 N: **a** 0 wt%; **b** 1 wt%; **c** 2 wt%; **d** 3 wt%

The EDS information of the typical MML for the 2 wt% CNT/6061Al composite is shown in Fig. 14. It indicated that the O element (Fig. 14b) and Cu element (Fig. 14c) were continuously induced into the MML, during the alternate stacking process of wear debris. The existence of O could weaken the adhesive strength of MML to some extent [45], which had a negative impact on the wear resistance of CNT/6061Al composites.

As the applied load increased to 60 N, the depth and width of ploughing significantly increased (Fig. 15a–d). Many larger microcracks (Fig. 15e–h) were observed in MML for CNT/6061Al composites, and the initiation location of microcracks accompanied with large voids. Especially, for the 3 wt% CNT/6061Al composite, the wear debris of counterpart material stacked on the MML had a much larger size. The debris with larger size would worsen the adhesive strength of MML, meanwhile the presence of microcracks and voids also weakened the property of anti-shearing strain of MML under a higher applied load [10]. Further, the thickness of MML gradually increased with increasing CNT concentration, which was contrary to those under 30 N. In general, the thin MML could effectively improve the wear resistance. Therefore, the wear rate increased as increasing the CNT concentration under 60 N.

### 4.3 Peeling Ways of Wear Debris

As mentioned above, the MML was composed of wear debris, which was formed due to the alternate stacking of the comminuted composites and counterpart materials during the wear process. The periodic reciprocating wear process had a great impact on the embedded CNT. To assess the peeling ways of wear debris on the wear behavior, the stress states imposed on CNT under different conditions were studied. As shown in the Raman Spectroscopic results (Fig. 16), the peakof the spectrum shifted to the lower value after the wear experiment under 30 N.

To the best of our knowledge, compressive stress would cause the peak moved toward higher Raman shift, and vice versa [46, 47]. For the raw CNT/6061Al composites, CNT would suffer compressive stress after cooling during quenching, because CNT had a much lower thermal expansion coefficient than the Al matrix. After the wear experiment under 30 N, the characteristic peak of 2 wt% and 3 wt% CNT/6061Al composites shift to lower peak position. That is, the compressive stress on CNT were released, and the stress state of CNTs changed under the shear stress effect, indicating the plastic deformation occurrence of wear surface in CNT/6061Al composites.

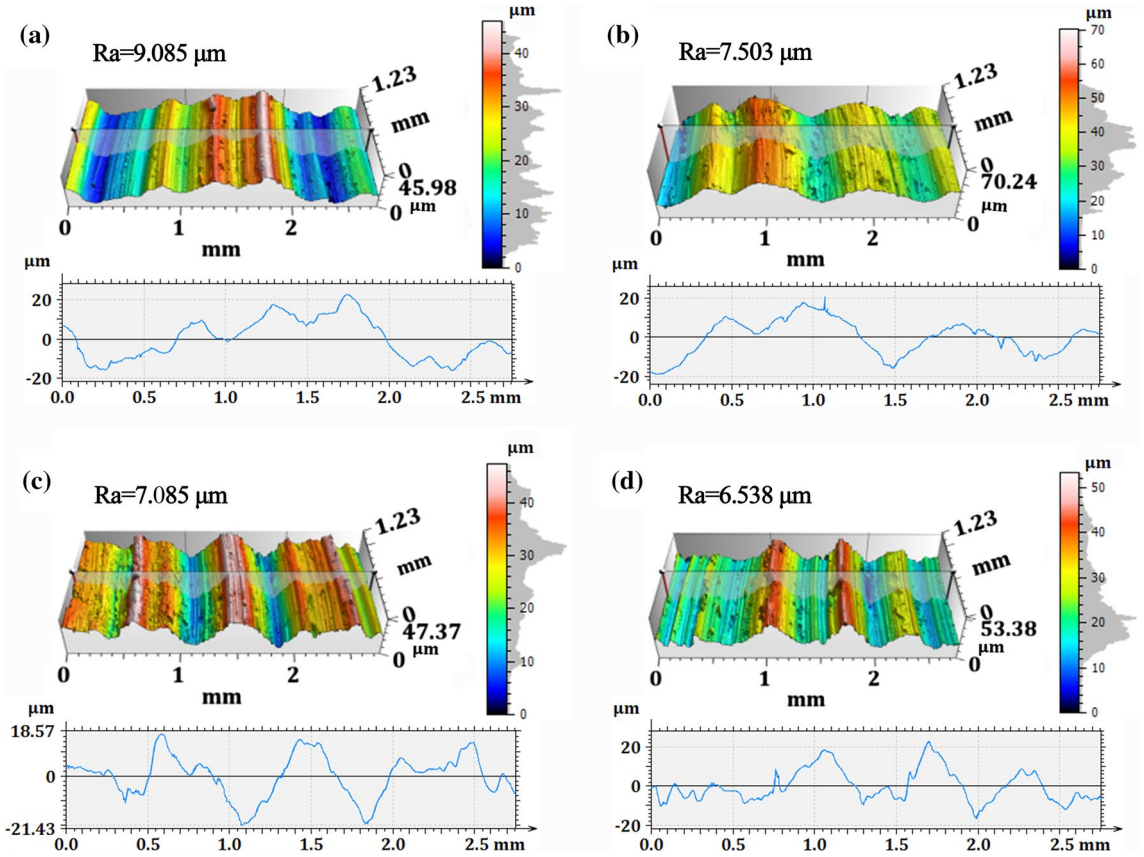


**Fig. 12** 3d profilogram of wear tracks for the CNT/6061Al composites with different CNT concentrations under 60 N: **a** matrix alloy; **b** 1 wt%; **c** 2 wt%; **d** 3 wt%

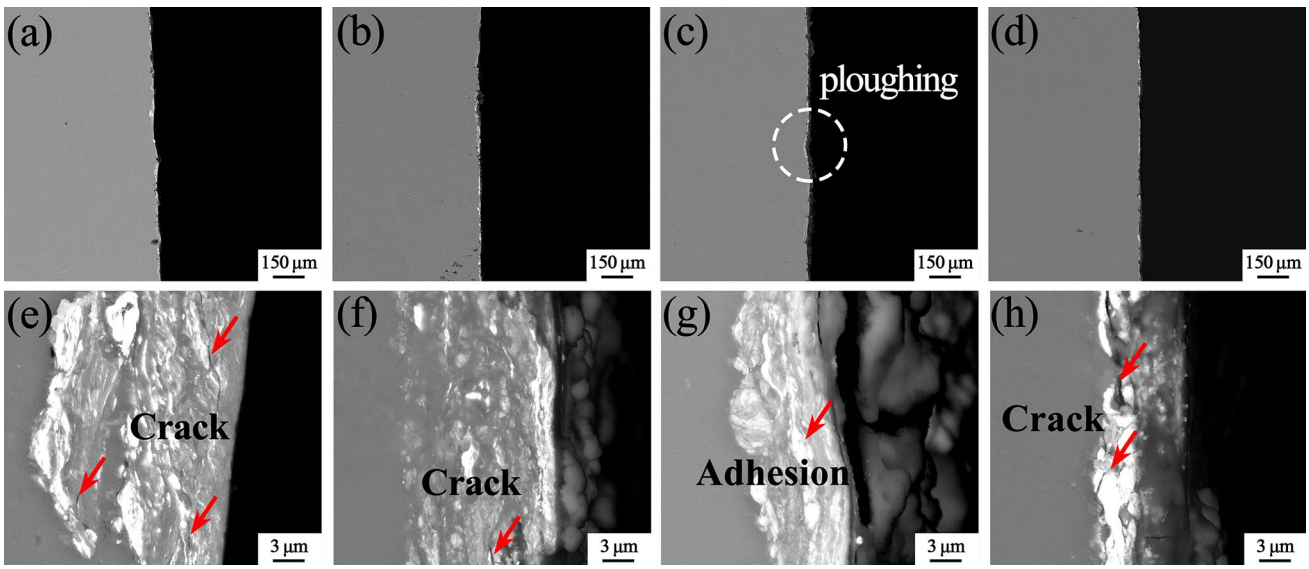


**Fig. 13** Wear subsurface cross sections of CNT/6061Al composites with different CNT concentrations under 30 N: **a**, **e** 0 wt%; **b**, **f** 1 wt%; **c**, **g** 2 wt%; **d**, **h** 3 wt%

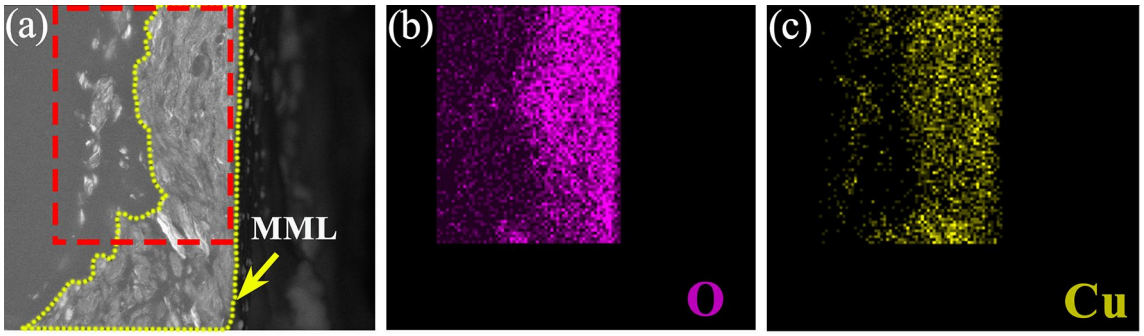


**Fig. 14** EDS analysis of the typical MML for the 2 wt% CNT/6061Al composite

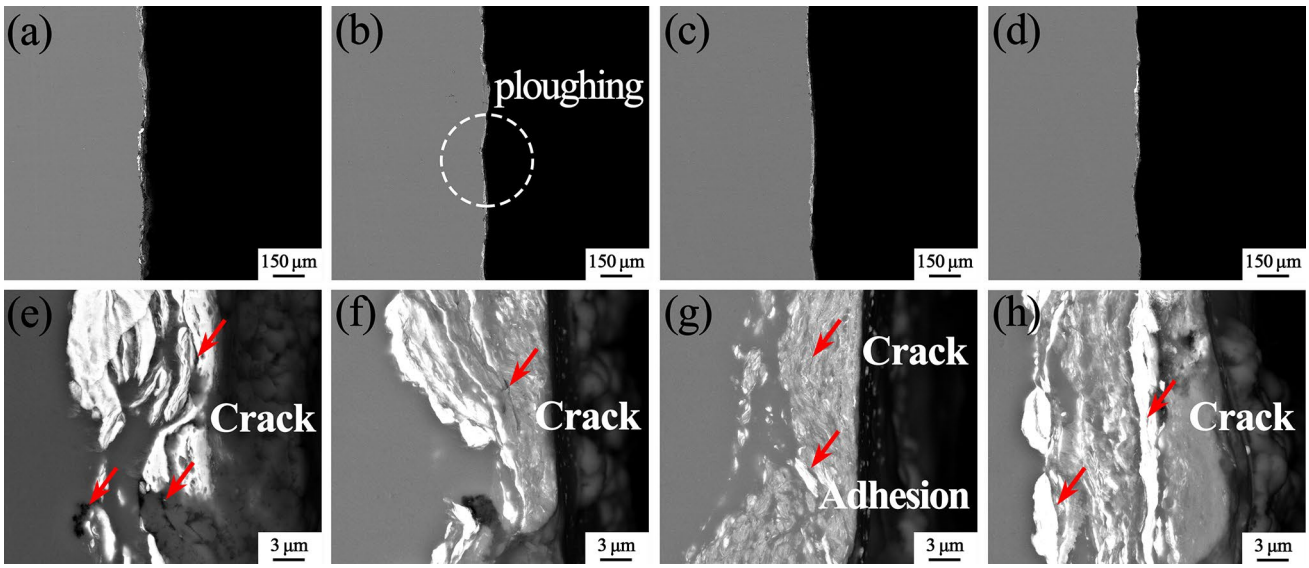


**Fig. 15** Wear subsurface cross section of CNT/6061Al composites with different CNT concentrations under 60 N: **a**, **e** 0 wt%; **b**, **f** 1 wt%; **c**, **g** 2 wt%; **d**, **h** 3 wt%

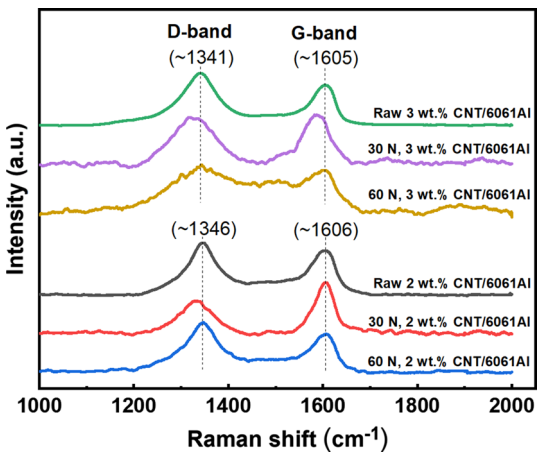


**Fig. 16** Raman spectra of the wear surfaces of 2 wt% and 3 wt% CNT/6061Al composites under 30 N and 60 N

But the peak shifting of the spectrum did not occur as the load increased to 60 N, indicating that the embedded CNT was still under the influence of compressive stress, and the compressive stress could not be effectively released during the wear process. As shown in Fig. 3b, the elongation of CNT/6061Al composites significantly decreased with increasing CNT concentration. It is believed that, the anti-shearing strain ability of CNT/6061Al composite was significantly weakened for the poor plasticity. The compressive stress kept on CNT after the wear process under 60 N indicated that the wear debris were peeled off from the wear surface directly and no obvious plastic deformation occurred for 3 wt% CNT/6061Al composite. So, the severe delamination wear occurred and the bigger size of wear debris formed, which resulted in severe wear loss.

## 5 Conclusions

1. HEM combined with powder metallurgy technology uniformly dispersed the CNT into the Al matrix. As a result, the vickers hardness increased significantly but the elongation decreased with increasing CNT concentration from 0 to 3 wt%.
2. Under 15 and 30 N load, the friction coefficient decreased first and then increased with increasing CNT concentrations. However, the friction coefficient decreased gradually with the increase in CNT concentration under the applied load of 60 N, as the result of the decreasing surface roughness and the occurrence of large but irregular wear debris.
3. Under the applied load of 15 N and 30 N, the wear rate decreased slightly first and then increased rapidly as the CNT concentration increased from 0 to 3 wt%. As the applied load increased to 60 N, the wear rate increased dramatically under high shear stress effect, due to the poorer plasticity of composite with higher CNT concentration.
4. The adhesive wear, abrasive wear were the dominated wear mechanism under 15 N and 30 N load for the CNT/6061Al composites, while albronze was chosen as the counterpart material. But the delamination wear was the dominated wear mechanism as the applied load increased to 60 N.

**Acknowledgements** This work was financially supported by the Key Research Program of Frontier Sciences, CAS (No. QYZDJ-SSW-JSC015), the National Natural Science Foundation of China (Nos. 51931009, 51871214 and 51871215), the Liao Ning Revitalization Talents Program (No. XLYC1902058) and the Youth Innovation Promotion Association CAS (No. 2020197).

### Declarations

**Conflict of interest** The authors state that no conflicts of interest exist.

## References

[1] K. Morsi, A.M.K. Esawi, S. Lanka, A. Sayed, M. Taher, Compos. Pt. A-Appl. Sci. Manuf. **41**, 322 (2010)
[2] S.R. Bakshi, V. Singh, K. Balani, D.G. McCartney, S. Seal, A. Agarwal, Surf Coat. Technol. **202**, 5162 (2008)
[3] L. Jiang, Z. Li, G. Fan, L. Cao, D. Zhang, Carbon **50**, 1993 (2012)
[4] Z.Y. Liu, B.L. Xiao, W.G. Wang, Z.Y. Ma, J. Mater. Sci. Technol. **30**, 649 (2014)
[5] H. Choi, J. Shin, B. Min, J. Park, D. Bae, J. Mater. Res. **24**, 2610 (2011)
[6] H. Choi, G. Kwon, G. Lee, D. Bae, Scr. Mater. **59**, 360 (2008)
[7] K. Zhao, Z.Y. Liu, B.L. Xiao, D.R. Ni, Z.Y. Ma, Acta Metall Sin.-Engl. Lett. **31**, 134 (2017)
[8] F. Mokdad, D.L. Chen, Z.Y. Liu, B.L. Xiao, D.R. Ni, Z.Y. Ma, Carbon **104**, 64 (2016)
[9] S.R. Bakshi, A. Agarwal, Carbon **49**, 533 (2011)
[10] H.J. Choi, S.M. Lee, D.H. Bae, Wear **270**, 12 (2010)
[11] R. Pérez-Bustamante, J.L. Bueno-Escobedo, J. Jiménez-Lobato, I. Estrada-Guel, M. Miki-Yoshida, L. Licea-Jiménez, R. Martínez-Sánchez, Wear **292**, 169 (2012)
[12] A.M. Al-Qutub, A. Khalil, N. Saheb, A.S. Hakeem, Wear **297**, 752 (2013)
[13] I.Y. Kim, J.H. Lee, G.S. Lee, S.H. Baik, Y.J. Kim, Y.Z. Lee, Wear **267**, 593 (2009)
[14] M.M.H. Bastwros, A.M.K. Esawi, A. Wifi, Wear **307**, 164 (2013)
[15] J.L. Jiang, H.Z. Wang, H. Yang, J.C. Xu, Trans. Nonferrous Met. Soc. China **17**, s113 (2007)
[16] S.M. Zhou, X.B. Zhang, Z.P. Ding, C.Y. Min, G.L. Xu, W.M. Zhu, Compos. Pt. A-Appl. Sci. Manuf. **38**, 301 (2007)
[17] M. Yildirim, D. Özyürek, M. Gürü, Fuller. Nanotub. Car. N. **24**, 467 (2016)
[18] D.A. Rigney, L.H. Chen, M.G.S. Naylor, A.R. Rosenfield, Wear **100**, 195 (1984)
[19] T. Kayaba, K. Kato, ASME. New York, pp. 45–46 (1979).
[20] M. Kerridge, J.K. Lancaster, Proc. R. Soc. Lond. Ser. A. Math. Phys. Sci **236**, 250 (1997)
[21] M.D. Pashley, J.B. Pethica, D. Tabor, Wear **100**, 7 (1984)
[22] A.K. Vijh, J. Mater. Sci. **10**, 998 (1975)
[23] J. Ferrante, D.H. Buckley, A S L E Trans. **15**, 18 (1972)
[24] W.X. Chen, J.P. Tu, L.Y. Wang, H.Y. Gan, Z.D. Xu, X.B. Zhang, Carbon **41**, 215 (2003)
[25] L.H. Chen, D.A. Rigney, Wear **105**, 47 (1985)
[26] Z.Y. Liu, B.L. Xiao, W.G. Wang, Z.Y. Ma, Carbon **50**, 1843 (2012)
[27] S.R. Bakshi, D. Lahiri, A. Agarwal, Int. Mater. Rev. **55**, 41 (2013)
[28] D. Singla, K. Amulya, Q. Murtaza, Mater. Today: Proc. **2**, 2886 (2015)
[29] B. Bhushan, F.E. Talke, J. Tribol. **113**, 225 (1991)
[30] M.A. Chowdhury, M.K. Khalil, D.M. Nuruzzaman, M.L. Rahaman, Mech. Eng. **11**, 53 (2011)
[31] B. Bhushan, A.V. Kulkarni, Thin Solid Films **278**, 49 (1996)
[32] X.N. Li, Z.Y. Liu, Y.N. Zan, B.L. Xiao, D.R. Ni, Q.Z. Wang, D. Wang, Z.Y. Ma, Wear behavior of the raw and pre-smashed carbon nanotubes reinforced 6061Al composites fabricated by powder metallurgy. Sci. China Technol. Sci. (2022) accepted.
[33] S.M. Mahdavian, Y.W. Mai, B. Cotterel, Wear **82**, 221 (1982)
[34] T. Kayaba, K. Kato, A S L E Trans. **24**, 164 (2008)
[35] J.R. Fleming, N.P. Suh, Wear **44**, 57 (1977)
[36] N.P. Suh, Wear **44**, 1 (1977)
[37] S.T. Oktay, N.P. Suh, J. Tribol-Trans, ASME **114**, 379 (1992)
[38] J. Kukutschová, V. Roubíček, K. Malachová, Z. Pavlíčková, R. Holuša, J. Kubačková, V. Mička, D. MacCrimmon, P. Filip, Wear **267**, 807 (2009)
[39] J. Denape, J. Lamon, J. Mater. Sci. **25**, 3592 (1990)
[40] B.H. Lee, Y.T. Keum, R.H. Wagoner, J. Mater. Process. Technol. **130**, 60 (2002)
[41] H. Jiang, R. Browning, J. Fincher, A. Gasbarro, S. Jones, H.J. Sue, Appl. Surf. Sci. **254**, 4494 (2008)
[42] A.M. Hassan, A.T. Mayyas, A. Alrashdan, M.T. Hayajneh, J. Mater. Sci. **43**, 5368 (2008)
[43] C.H. Yin, Y.L. Liang, Y. Liang, W. Li, M. Yang, Acta Mater. **166**, 208 (2019)
[44] T. Lee, J. Lee, D. Lee, I. Jo, S.K. Lee, H.J. Ryu, J. Alloy. Compd. **831**, 154647 (2020)
[45] B. Venkataraman, G. Sundararajan, Wear **245**, 22 (2000)
[46] S. Reich, H. Jantoljak, C. Thomsen, Phys. Rev. B **61**, 13389 (2000)
[47] O. Lourie, H.D. Wagner, J. Mater. Res. **13**, 2418 (2011)